Modeling of Specific Lipopolysaccharide Binding Sites on a Gram-Negative Porin

Anusha Kesireddy,† Karunakar R. Pothula,† Jumin Lee,‡ Dhilon S. Patel,‡

Monisha Pathania,¶ Bert van den Berg,¶ Wonpil Im,*,‡ and Ulrich

Kleinekathöfer*,†

†Department of Physics and Earth Sciences, Jacobs University Bremen, 28759 Bremen, Germany

‡Departments of Biological Sciences and Bioengineering, Lehigh University, Bethlehem, PA
18015, USA

¶Institute for Cell and Molecular Biosciences, The Medical School, Newcastle University,

Newcastle upon Tyne NE2 4HH, United Kingdom

E-mail: woi216@lehigh.edu; u.kleinekathoefer@jacobs-university.de

Abstract

Protein-lipopolysaccharide (LPS) interactions play an important role in providing a stable outer membrane to Gram-negative bacteria. However, the LPS molecules are highly viscous, and sampling LPS motions is thus challenging on a microsecond timescale in simulations. To this end, we introduce a new protocol to randomly allow the LPS molecules to self-assemble around the protein and thereby reduce the starting bias in the simulations. Here we present all-atom molecular dynamics simulations of the OmpE36 porin in an outer membrane model which sum up to a simulation time of more than 20 μ s, and identify the geometrical properties of the first LPS shell and the role of calcium ions in LPS binding to the protein. The simulations reproduce LPS binding to the porin observed in a recently determined crystal structure, but not as compact as in the crystal structure. In addition, the influence of the outer membrane environment on the protein dynamics was analyzed. Our findings highlight the role of divalent cations in stabilizing the binding between proteins and LPS molecules in the outer membrane of Gram-negative bacteria.

1 Introduction

Gram-negative bacteria have an asymmetric outer membrane (OM) with phospholipids in the inner leaflet and lipopolysaccharides (LPS) in the outer leaflet. ^{1,2} LPS, the signature lipoglycan of the Gram-negative bacterial OM, have crucial implications on the antibiotic resistance, ³ virulence, host cell adhesion ⁴ and most particularly on the integrity of the OM. ^{5,6} LPS molecules are negatively charged lipoglycans composed of a highly conserved hydrophobic lipid A, a hydrophilic core oligosaccharide, and an repeating O-antigen polysaccharide specific to the bacterial serotype. Thus, the outer leaflet is rather complex and poses a tighter permeation barrier than the inner leaflet composed of unsaturated phoshoplipids ⁷ that, in contrast to the inner leaflet, also holds for hydrophobic molecules. The OM proteins (OMPs) inserted into the OM regulate influx and efflux of nutrients and antibiotics in and out of the bacterial cell. The integration of these proteins and lipids into the OM is essen-

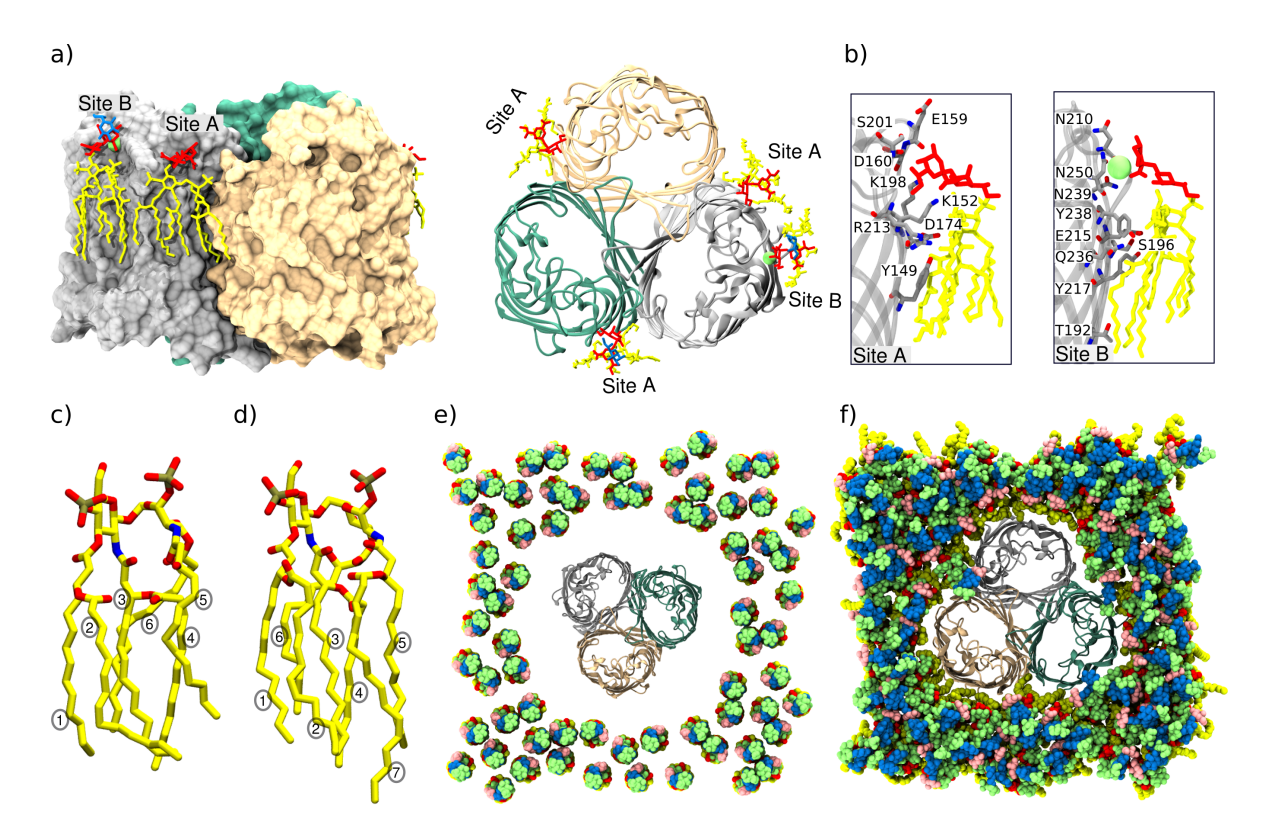


Figure 1: Binding features of the OmpE36-LPS complex. a) Side (left panel) and top views (right panel) of the OmpE36 crystal structure including two LPS molecules attached to its surface. The components of LPS are shown in different colors, i.e., lipid A in yellow, Kdo (3-deoxy-D-manno-oct-2-ulosonic acid) in red, and Hep (L-glycero-D-manno-heptose) in blue. The Ca²⁺ ion at the LPS site B is shown as a green sphere. b) Snapshots of site A (left panel) and site B (right panel) porin residues interacting with Kdo and lipid A units in the crystal structure. Structural models of lipid A in c) hexa-acylated and d) hepta-acylated LPS molecules are shown in stick representation. e) Top view of the starting system in one of the hexa-acylated systems, where lipids are placed 2 nm away from the protein. f) OmpE36 system embedded in a hexa-acylated LPS bilayer built in a traditional way by placing lipids next to protein. The components of LPS are represented with different colors; lipid A in yellow, Kdo in red, Hep in green, Gal (galactose) in pink and Glc (glucose) in blue. For clarity, water and ions are not shown.

tial to maintain the OM impermeability, which is largely attributed to non-covalent lateral interactions between proteins and lipids. Additionally, the assembly and function of these OMPs relies strongly on the presence of LPS. ^{6,8–10}

As the OM provides a permeability barrier to antibiotics, biochemical and biophysical studies of the OM, especially of its essential component LPS, are of significant interest. Much progress has been made in the characterization of the enzymatic steps of LPS synthesis and

mechanistic details of LPS transport from the inner to the outer membrane. ^{11,12} Furthermore, LPS binding to various OM channels have been reported by several biochemical ^{13–16} and structural studies, ^{17,18} leading to hypotheses on their possible involvement in folding and assembly of these channels in the OM. However, specific interactions and the stoichiometry of the annular lipid shell around the OMPs is currently somewhat obscure. Moreover, the influence of the asymmetric OM on the structure-dynamics-function of the OM channels is yet to be understood in detail. A better understanding of structural models of OMP-LPS complexes thus might provide clues to target the structural integrity of the OM.

To this end, molecular dynamics (MD) simulations have proven to be very insightful in simulating membrane protein-lipid complexes and previously have been employed to examine the specific interactions between OMPs and LPS 19 and the influence of LPS on the dynamics of the OMPs. ^{20–26} However, because the diffusion rate of LPS molecules in a bilayer is slow compared to phospholipids, the LPS molecules are highly localised on a time scale of 100 ns to 10 μ s. Hence, the results are potentially highly biased by system preparation and placement of LPS molecules around the OMPs in the starting system. Here, we introduce a new protocol for the LPS simulations to avoid the bias in the starting conformation and investigated the OmpE36 trimeric OMP, which is a major porin in the OM of Enterobacter cloacae. The structure forms a 16 β -stranded porin and shares structural features with its ortholog OmpC from Escherichia coli (Figure 1a). Based on the recent X-ray structure, two specific LPS binding sites per monomer have been defined: site A is positioned on loop L4 and present at the interface of two monomers and site B is positioned at loop L5 adjacent to the former (Figure 1b). The latter requires a divalent cation to stabilize its interaction with OmpE36. 18 Here we examined the stoichiometry and the role of calcium ions in LPS binding to OmpE36 porin. Furthermore, we compared the behavior of OmpE36 in different OM bilayers and a phospholipid bilayer.

2 Methods

2.1 Outer membrane system setup

Molecular simulation systems of OmpE36 (PDB: 5FVN) embedded in two different OM bilayers, i.e., hexa-acylated and hepa-acylated LPS, mimicking the E. coli OM have been prepared. The hexa-acylated K-12 LPS is the most common type found in E. coli OM and the hepta-acylated K-12 LPS is a rare chemotype but found in the crystal structure of OmpE36. The K-12 core region is composed of oligosaacharide sugars such as Kdo (3-deoxy-D-mannooct-2-ulosonic acid), Hep (L-qlycero-D-manno-heptose), Gal (galactose) and Glc (glucose). The chemical differences in the lipid A of hexa- and hepta-acylated chains are shown in Figures 1c-d. The inner leaflet is composed of 1-palmitoyl(16:0)-2-palmitoleoyl(16:1 cis-9)phosphatidylethanolamine (PPPE), 1-palmitoyl(16:0)-2-vacenoyl(18:1 cis-11)-phosphatidylglycerol (PVPG), and 1,1'-palmitoyl-2,2'-vacenoyl-cardiolipin with a net charge of -2e (PVCL2) at a ratio of 15:4:1. A similar composition of the OM has been used in the previous simulations of OmpF²⁰ and OmpLA.²⁵ Calcium ions were placed near LPS regions to neutralize LPS, and 1 M KCl salt was added to the bulk region in the system. Ten replica systems were built independently for hexa-acylated and hepa-acylated LPS systems for better sampling of the protein-lipid interactions. These systems were built by placing the lipids 2 nm away from the protein (Figure 1e) by following the protocols in the CHARMM-GUI Membrane Builder. 27-30 After the minimization of 1,000 steps, the systems were equilibrated in two steps to allow the packing of lipids around the protein. A 10-ns equilibration in an NPT ensemble (Berendsen barostat and thermostat³¹) with a time-step of 1 fs was first performed. Subsequently, a 500-ns equilibration with restraints on the backbone of protein was carried out in an NPT ensemble using a time-step of 2 fs and semi-isotropic coupling to a Parrinello-Rahman barostat 32 at 1 bar with a coupling constant of 5 ps. The temperature was set to 300.15 K using a Nosé-Hoover thermostat ^{33,34} with a coupling constant of 1 ps. During the equilibration, z axis restraints were applied on the phosphorus atoms to maintain the plane of the membrane relative to the protein. The final production simulations were performed

for 500 ns in similar conditions, but without restraints on the protein. During the equilibration and production runs, ^{20,25} dihedral angle restraints were applied on all the LPS sugar residues to maintain the specific chair conformation of sugar rings.

As a reference to compare the new protocol, we further built three systems of the OmpE36 porin embedded in a hexa-acylated bilayer with lipids placing next to the protein (Figure 1f) and added LPS-neutralizing calcium and 1 M KCl solution using CHARMM-GUI Membrane Builder. The equilibration was performed for a total of 450 ps in NVT and NPT ensemble by gradually reducing the restraints to zero on LPS, phospholipids and water molecules. The final production simulations were performed for 500 ns in an NPT ensemble, achieved by semi-isotropic coupling to a Parrinello-Rahman barostat 32 at 1 bar with a coupling constant of 5 ps. The temperature was set to 300.15 K using a Nosé-Hoover thermostat 33,34 with a coupling constant of 1 ps. Again dihedral angle restraints were applied on all the LPS sugar residues.

2.2 Modified parameters for the calcium ions

To test the influence of the calcium charge on LPS binding, the equilibrated structure of all replicas of the hexa- and hepta-acylated LPS systems from the new protocol were simulated for 1 ns with the calcium charge artificially set to zero in a NVT ensemble. Positional restraints were applied on the heavy atoms of the protein to maintain a stable secondary structure and z axis restraints on the 30 heavy atoms within each LPS molecule.

Furthermore, we tested the impact of altering the calcium non-bonded Lennard-Jones parameters (NBFIX) with acetate groups of aspartate and glutamate residues to values recently proposed. Instead of starting new system set-ups from scratch, here, we selected five replicas of the equilibrated hexa-acylated systems based on the new protocol and resampled the calcium ions after closely packing the LPS around the protein in four steps. In the first step, the charge of calcium is artificially set to zero to remove the neutralizing effects of calcium ions in a NVT ensemble for 500 ps by freezing the positions of all atoms of the protein and membrane. Subsequently, the lipids molecules are released in the membrane

plane to allow for close packing around the restrained protein due to negatively charged LPS-LPS repulsion in the absence of neutralizing calcium ions for 1 ns in a NVT ensemble followed by resetting the calcium charge to +2e and simulating for 500 ps (NVT) and 1 ns (NPT) to allow the calcium ions to move into LPS regions by restraining the protein and membrane in all directions. Close to 30 heavy atoms within each LPS molecule and all-heavy atoms of the protein were selected to keep restraints during this procedure. Finally, the five replicas were simulated for 100 ns without the restraints on the protein and membrane in the NPT ensemble with the other parameters similar to those of the final conventional LPS simulations.

2.3 DMPC bilayer systems

For the comparison of the porin dynamics in different membrane systems, we additionally built three DMPC bilayer systems with OmpE36 protein and equilibrated in a step wise manner with the CHARMM-GUI default protocol for membrane systems and simulated each for 500 ns in the NPT ensemble with parameters similar to final LPS simulations.

2.4 Molecular dynamics simulations

All MD simulations of the LPS systems were carried out with GROMACS 5.2 and of the DMPC systems with GROMACS 4.6.5³⁶ using the all-atom CHARMM36 force field for proteins, ³⁷ lipids, ³⁸ carbohydrates, ^{39–42} LPS ^{43,44} and the CHARMM TIP3P water model. ⁴⁵ The long-range Coulombic interactions were treated using the particle mesh Ewald (PME) method ⁴⁶ with a short-range cutoff of 1.2 nm, whereas Lennard-Jones interactions were considered up to a distance of 1.0 nm, and a switch function was used to smoothly turn off the interactions to reach zero at 1.2 nm. A time step of 2 fs was employed in the simulations by applying constraints on the bonds containing hydrogen atoms using the LINCS algorithm. ⁴⁷

3 Results and Discussion

3.1 New protocol for LPS simulations

Our main aim in this study is to investigate the OmpE36-LPS interactions. However, LPS lipids are highly viscous, and sampling the LPS motions is very challenging on submicrosecond time scales even if one would use a coarse-grained representation. Thus, the final results could be highly dependent on the initial structure. For instance, in three independent hexa-acylated LPS simulations, when LPS molecules were initially placed next to OmpE36 (Figure 1f), the LPS molecules in the outer layer show no lipid diffusion (Figure S1) and lack motional sampling on the 500-ns time scale. To avoid such a bias in the LPS systems, we used a randomizing approach to construct the initial structure by allowing the OM to (semi-)self-assemble around the porin. For better statistics, ten replicas for each of the hexa-acylated and hepta-acylated LPS systems were prepared independently by placing the lipids 2 nm away from the porin (Figure 1e) in the inner and outer leaflet and equilibrated for 500 ns in an NPT ensemble to form a bilayer and an annular shell around the porin as shown in density plots in Figures S2 and S3. After the self-assembly of the OM, we further extended the simulations for 500 ns without any restraints on protein and analyzed the OmpE36-LPS interactions. The root mean square deviations (RMSDs) of the C_{α} atoms measured for protein structural changes converge after about 100 ns to values of 0.1-0.2 nm in each of the simulations (Figure S4).

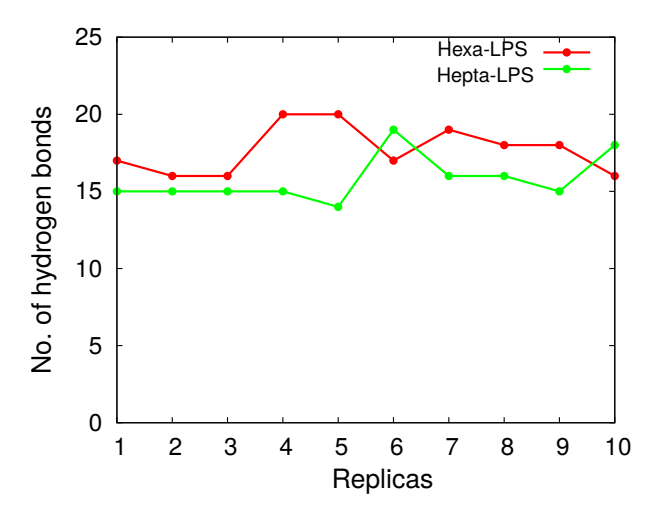


Figure 2: Number of LPS molecules forming at least one (log-lived or short-lived)hydrogen bond with the trimeric OmpE36 protein in the ten replica systems.

3.2 Lipid arrangement around the OmpE36 porin

As a first step, we investigated the stoichiometry of LPS molecules in the annular shell of OmpE36 by monitoring the hydrogen bond interactions of each LPS molecule with the protein. In the ten hexa-acylated replicas, out of 69 LPS molecules in the cubic box, 16 to 20 LPS molecules are found to form hydrogen bond interactions with the trimeric protein (Figure 2), ranging from short-lived to long-lived interactions, and form an annular shell around the protein. Similarly in the hepta-acylated systems, 14 to 19 LPS molecules form hydrogen bonds with the protein and this slight reduction in the annular shell is probably due to the extra acylated chain in hepta-acylated LPS molecules. The observed differences between the independent simulations of the same system are not surprising considering the fact that LPS binding to the protein is rather a dynamic process. Since LPS conformations are highly flexible, they can have many orientations to interact with the protein and thus the stoichiometry can vary even on finite simulation time scales. Our results show at least 15 LPS molecules are forming hydrogen bonds consistently in all trajectories and, moreover, most of these interactions persist throughout the simulations indicating the existence of several preferential binding sites of LPS molecules on the surface of the protein, i.e., more than the two sites observed in the crystal structure.

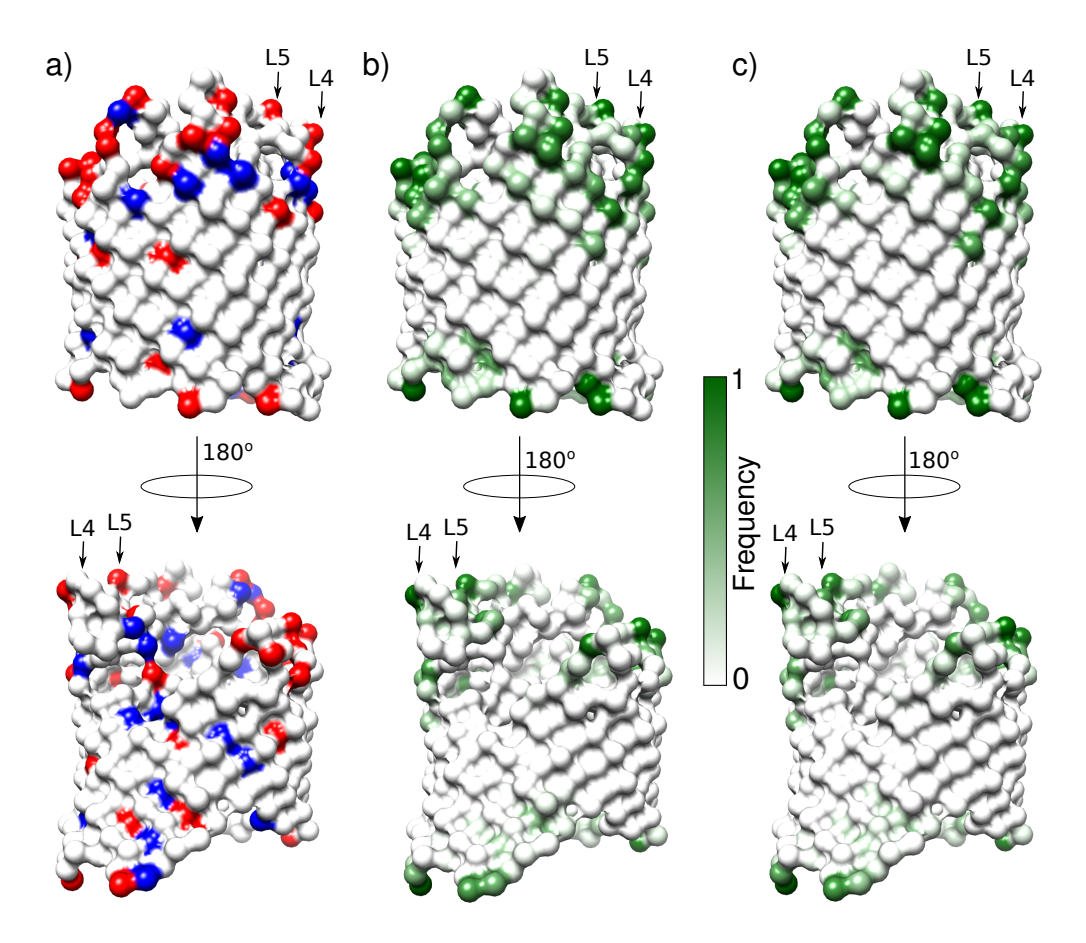


Figure 3: a) Distribution of positive (blue) and negative (red) residues on the protein surface oriented towards the membrane interface (upper panel) and towards the protein trimer interface (lower panel). The calcium interactions with each residue in b) hexa-acylated replicas and c) hepta-acylated replicas are shown on the surface of protein. The color scale corresponds to the normalized probability of the calcium interactions in all replicas.

3.3 Influence of calcium on the LPS binding

A LPS-containing OM bilayer requires divalent cations, like calcium, to neutralize the electrostatic repulsion between the negatively charged LPS molecules and to provide stability to the OM. The Figures S2 and S3 show that the calcium ions are highly localized in the vicinity of the phosphate groups to cross-link the LPS molecules. In addition, the calcium ions are strongly attracted towards electronegative positions around the protein. This finding is consistent with the charge distribution on the outer surface of the protein as it contains more negatively than positively charged residues towards the extracellular side (Figure 3a). We monitored the occupancy of calcium ions within 0.5 nm of each residue in all trajectories and

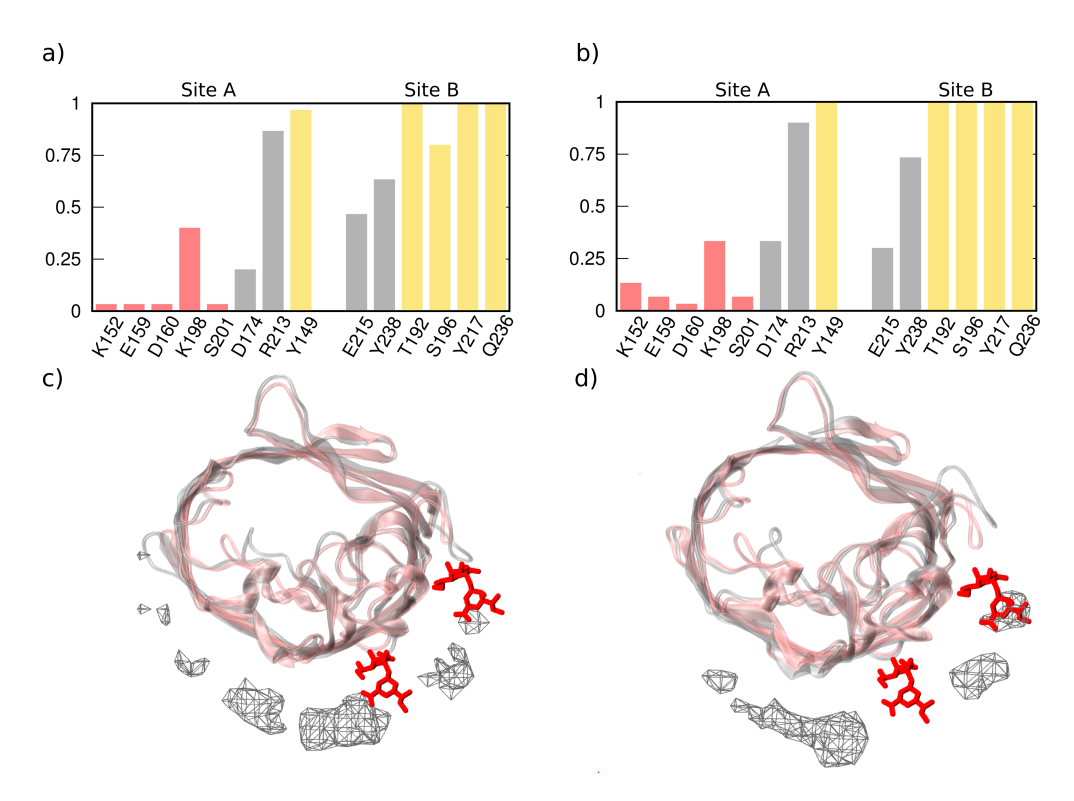


Figure 4: Interaction analysis of the site A and site B residues with LPS molecules. a, b) Normalized contact frequency between the corresponding residues and LPS components (red: Kdo, gray: lipid A head group, yellow: lipid A acylated chains) in the last frames of the ten replicas of the hexa- and hepta-acylated systems with a standard calcium charge as of +2e. c, d) Comparison of averaged Kdo occupancy (represented as grid of the electron density with isovalue 0.14) for the last MD frames of the ten replicas of the hexa- and hepta-acylated systems compared to the crystal structure Kdo positions (red sticks). The porin monomer from the crystal structure is shown in reddish color while one of the MD end structures is overlayed in gray. For the contact and occupancy analysis, we considered residues within a distance of 0.35 nm to the respective LPS groups.

found that negatively charged residues, particularly towards the extracellular side, strongly and consistently interact with calcium ions (Figures S5 and S6). The probability of a calcium occupancy on the surface of the protein in the hexa- and hepta-acylated systems is shown in Figures 3b,c and the interactions are consistent in both OM bilayers. With such a high occupancy towards the extracellular region, the calcium ions play an important bridging role in mediating the interactions between the negatively charged LPS groups (like Kdo and lipid A head group) and the respective protein residues.

Furthermore, we assessed how our simulations could reproduce the crystallographic contacts of lipid A and Kdo groups at sites A and B with the porin. We investigated the

probability of a contact within 0.35 nm of site A and site B residues with lipid A and Kdo components in all replicas. The site A and B residues which are found to interact with the lipid A and the Kdo residues in hexa-acylated systems are shown in Figure 4a. The direct interactions between lipid A tail with site A and site B residues are persistent in most of the replicas followed by lipid A head and to a much lesser extent Kdo residues interact with site A and site B residues. A similar trend of interactions is observed in the hepta-acylated systems (Figure 4b). These results indicate that LPS molecules are able to reach the site A and B residues on the surface of the protein, but the calcium ions compete with Kdo and lipid A head groups to interact with the negatively charged residue on the extracellular side of the porin.

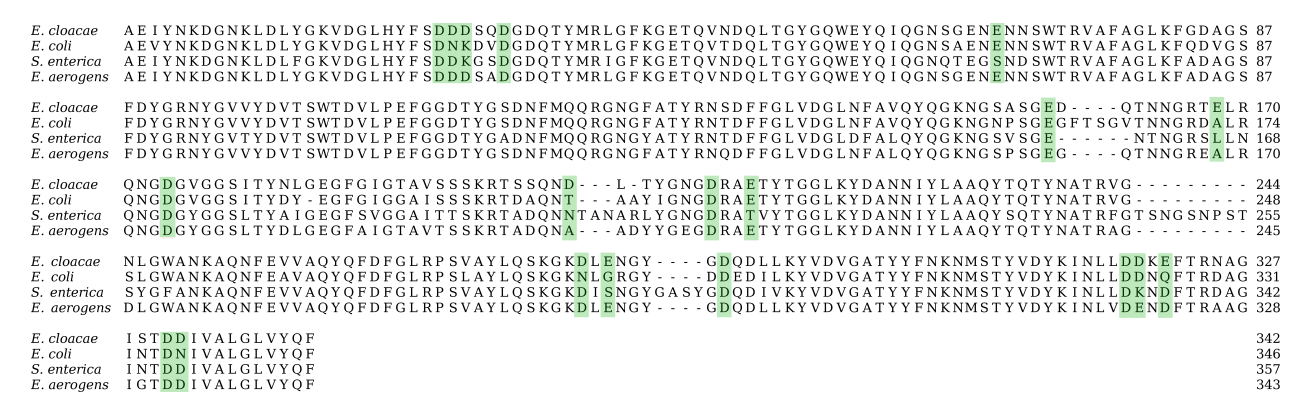


Figure 5: Sequence analysis of OmpC homologues from *Enterobacter* species *cloacae* and *aerogenes*, *Escherichia coli* and *Salmonella enterica*. The OmpE36 negatively charged residues interacting with calcium ions for more than 50 % of probability are highlighted by green boxes showing their conservation among other species.

Moreover, we analyzed the conservation of these calcium interacting residues in OmpE36 homologue sequences in *Enterobacter* species *cloacae* and *aerogenes*, *Escherichia coli and Salmonella enterica*. The sequence alignment was performed using Jalview. ⁴⁸ The calcium interacting residues observed for OmpE36 are mostly conserved in these organisms as shown in Figure 5. The evolutionary conservation of calcium binding residues suggest a functional role for calcium in stabilizing the OMP-LPS complexes. These findings highlight the role of divalent ions in stabilizing the LPS-OMPs complex in the OM of Gram-negative bacteria.

3.4 Modified calcium parameters

The observation that the contacts between LPS molecules and protein residues in the hydrophobic region are more prominent than in the hydrophilic region led us to investigate the effect of calcium in the OmpE36-LPS interactions. To test the influence of calcium on LPS binding, we performed several extended simulations by neutralizing the calcium charge, i.e., artificially setting the ionic charge to zero. Interestingly, when the calcium is neutralized in a 1-ns trajectory, the LPS molecules, particularly charged groups of LPS molecules, seem to come much closer to the protein as in the crystal structure. As shown in Figures 6a-b, the frequencies of the site A and B interactions are higher with Kdo and lipid A head groups compared to simulations with default calcium charge. The Kdo groups show tight packing with the porin and match the occupancies of Kdo at site A and site B as in the crystal structure (Figures 6c-d). Further, we investigated the LPS binding with improved calcium force fields in five replicas of hexa-acylated systems. However, the interaction frequencies of Kdo and lipid A head groups with site A and site B do not seems to change significantly (Figure S7). Despite the improvement of the non-bonded parameters (NBFIX) for calcium ions interacting with acetate groups of aspartate and glutamate residues, the calcium ions are still strongly attracted to regions on the surface of the porin similar to those obtained with the unmodified CHARMM36 force field parameters (Figure S8).

3.5 Protein dynamics: LPS vs DMPC bilayer

In addition to the simulations with LPS-containing OMs, we simulated OmpE36 in a DMPC bilayer (3 x 500 ns) to compare the influence of the lipid environment on the protein dynamics. Figure 7 shows the average root-mean-square-fluctuation (RMSF) of the protein in different membrane environments. Here we focused our analysis on the three major loops, i.e., the constriction loop L3 and the two extracellular loops L4 and L5 which interact with sites A and B. The two extracellular loops L4 and L5 make a number of polar interactions with the co-crystallized LPS molecules in the crystal structure. Loop L3 which has no direct contact to the lipid environment shows a slightly higher flexibility in the LPS bilayers which

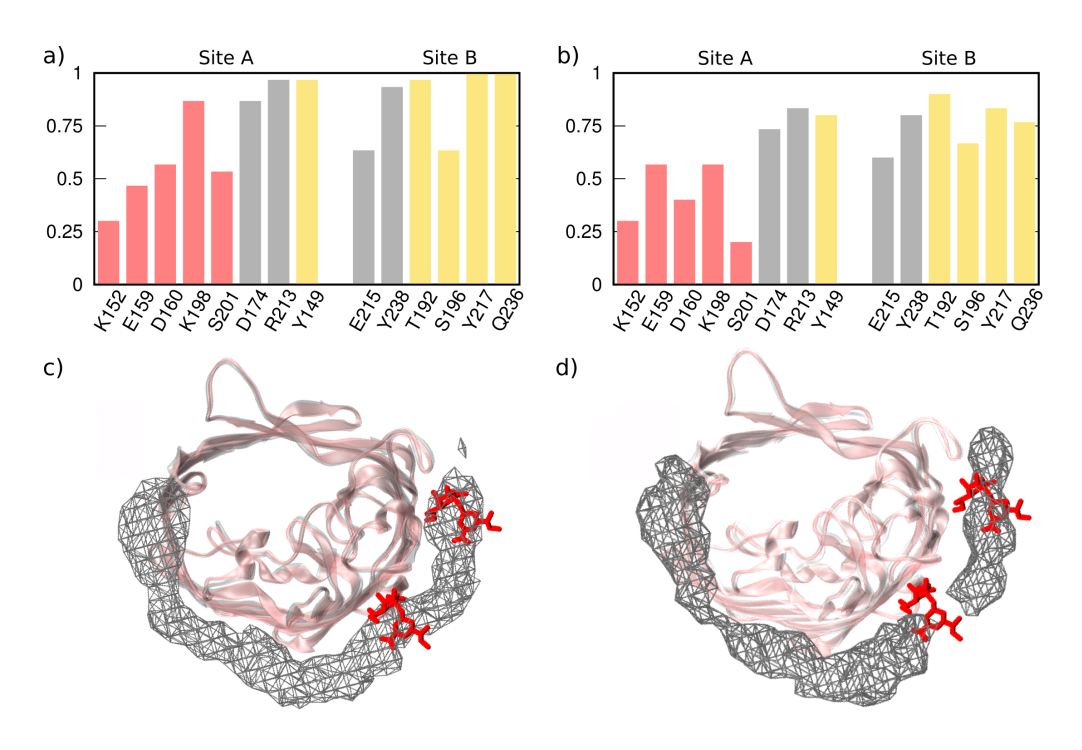


Figure 6: Same as Figure 4 but with neutralized calcium ions.

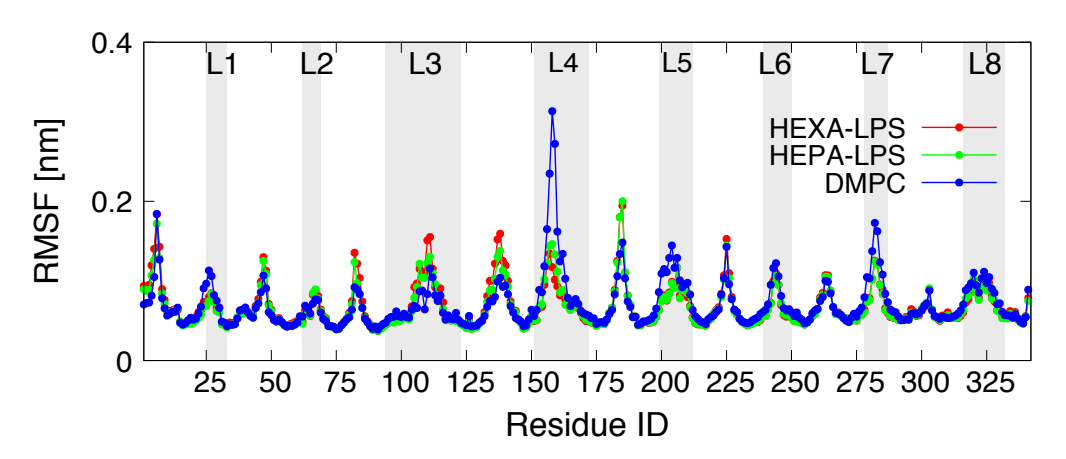


Figure 7: Comparison of protein dynamics in different lipid bilayers. Average $C\alpha$ RMSF plot of the OmpE36 protein in two different LPS and in a DMPC bilayer calculated from the last 350 ns of the MD trajectories. Each line represents the average of 30 monomers in the respective bilayer.

might be propagated by the membrane-interacting β -strands between loops L3 and L4. This region, which partially consists of an α -helix and a turn coil, is located inside the lumen of the pore. In previous MD simulations, 20,49 it has been shown that loop L3 of OmpF is highly flexible in a phospholipid and a LPS bilayer and the flexibility varies with the protonation of residues belonging to the constriction region. In general, the flexibility of this

loop determines the functional properties of the porins. Loop L4 shows the largest variation in the dynamics between the LPS and DMPC membrane environments. Loop L4 present at the interface between the two monomers is highly mobile in the DMPC membrane. In the presence of LPS, OmpE36 is fully constrained by the LPS matrix, and in particular loop L4 is surrounded by inner core Kdo and Hep sugar molecules as well as by calcium ions. This observation is consistent with the crystal structure where loop L4 is surrounded by LPS A. ¹⁸ Loop L5, which is adjacent to loop L4, also shows slightly higher flexibility in the DMPC bilayer. Moreover, a similar behavior can be seen for the extracellular loop L7. This comparison highlights the importance of LPS to restrict the flexibility of the protein at the extracellular side in a similar manner as shown for OmpF earlier. ²⁰

4 Conclusions

Lipids interact specifically with membrane proteins and modulate their functional activity. However, studying the interaction between LPS and OMPs of Gram-negative bacteria is challenging due to slow diffusion of LPS in MD simulations. To this end, we introduced a new protocol to allow the LPS molecules to self-assemble around the OMP and thereby reduced the starting bias in the system to study the structural and functional properties of OmpE36. Lipid/protein stoichiometries have been determined experimentally for several β -barrel proteins of Gram-negative bacteria. Ramakrishnan et al. ⁵⁰ determined stoichiometries of 11 and 32 dimyristoylphospatidylglycerol (DMPG) lipids for OmpA and FhuA, respectively, using electron spin resonance spectroscopy. Marsh and coworkers ^{51,52} developed a simple geometric model to determine the stoichiometries of the first lipid shell of phospholipids around β -barrel OMPs. However, the approach does not seem to be a satisfactory quantitative method to determine the stoichiometry of protein-lipid interactions.

Protein purification studies of an OmpF-LPS complex reported a stoichiometry of 9 LPS per OmpF trimer. ¹⁶ Recently, the extended ladder on SDS/PAGE in the presence of excess amounts of LPS demonstrated the existence of several LPS binding sites on OmpF. ¹⁸ In addition, a FhuA-LPS complex structure showed a single LPS bound to the barrel, ¹⁷ whereas

the recent OmpE36-LPS structure showed four LPS molecules bound to a trimer. ¹⁸ So far, the available biochemical and structural data on the OMP-LPS studies showed no definite stoichiometry. In our modeling strategy, we filled a finite volume around the trimer with the 69 LPS molecules in the outer leaflet and simulated using periodic boundary conditions. In both simulations with hexa- and hepta-acylated LPS, we observed that at least five LPS molecules per monomer are forming hydrogen bond interactions.

Interestingly, the LPS molecules roughly reached the positions close to sites A and B as in the crystal structure and showed more frequent interactions with the lipid A tails than with the charged lipid A head groups and Kdo components. Since the porin OmpE36 has many negatively charged residues on the extracellular side, many calcium ions diffuse into these electronegative regions during the simulations and were sitting close to the carboxylate or polar groups, impeding the direct interaction between porin and LPS molecules, particularly towards the extracellular side. Calcium-mediated OMP-LPS interactions have been studied for a long time, but the details are usually limited to ethylenediaminete-traacetic acid (EDTA) chelation studies. Excess amounts of CaCl₂ or MgCl₂ increase the bands of the OmpF-LPS complex in SDS/PAGE experiments, ¹⁸ implying a metal concentrationdependent LPS binding to the OMP. From the structural perspective of OmpE36, it is reasonable for calcium ions to bridge interactions between the negatively charged LPS groups and the protein residues, otherwise the repulsion between negatively charged groups on the protein and in LPS molecules would render the OM unstable. In short simulation tests with neutralized calcium ions, we observed an increase in the direct contacts of LPS molecules with site A and B residues. These tests indicate that the close contacts found in the crystal structure could be due to crystal artifacts or lower calcium concentration in the experiments and this might explain the disparity between the interactions in the crystal structure and the MD simulations.

Supporting Material

Eight figures are available as supporting material.

Author Contributions

W.I. and U.K. designed this study. A.K., K.R.K., J. L., and W.I. set up and run the simulations. A.K. K.R.K., W.I. and U.K. analyzed the data with input from D.S.P, B.v.d.B. and M.P. The manuscript was written by A.K., K.R.K., W.I. and U.K. with input from all authors.

Acknowledgements

The research of A.K., K.R.K., B.v.d.B., and U.K. has received support from the Innovative Medicines Joint Undertaking under Grant Agreement No. 115525, resources which are composed of financial contribution from the European Union's seventh framework programme (FP7/2007-2013) and EFPIA companies in kind contribution. M.P. is a Marie Skłodowska-Curie fellow within the "ITN Translocation" Network, project No. 607694. In addition, the work was supported in part by grants from the NSF MCB-1727508, NSF MCB-1810695, and XSEDE MCB070009, as well as Friedrich Wilhelm Bessel Research Award from the Humboldt foundation (to WI).

References

- (1) Nikaido, H.; Vaara, M. Molecular Basis of Bacterial Outer Membrane Permeability.

 Microbiol. Rev. 1985, 49, 1, DOI: 10.1128/MMBR.67.4.593-656.2003.
- (2) Nikaido, H. Molecular Basis of Bacterial Outer Membrane Permeability Revisited. *Microbiol. Mol. Biol. Rev.* **2003**, *67*, 593–656, DOI: 10.1128/MMBR.67.4.593-656.2003.
- (3) Delcour, A. H. Outer Membrane Permeability and Antibiotic Resistance. *Biochim. Bio-phys. Acta, Proteins Proteomics* **2009**, *1794*, 808–816, DOI: 10.1016/j.bbapap.2008. 11.005.
- (4) Day, C. J.; Tran, E. N.; Semchenko, E. A.; Tram, G.; Hartley-Tassell, L. E.; Ng, P.

- S. K.; King, R. M.; Ulanovsky, R.; McAtamney, S.; Apicella, M. A. et al. Glycan:Glycan Interactions: High Affinity Biomolecular Interactions That Can Mediate Binding of Pathogenic Bacteria to Host Cells. *Proc. Natl. Acad. Sci. USA* **2015**, *112*, E7266–E7275, DOI: 10.1073/pnas.1421082112.
- (5) Putker, F.; Bos, M. P.; Tommassen, J. Transport of Lipopolysaccharide to the Gram-Negative Bacterial Cell Surface. FEMS Microbiol. Rev. 2015, 39, 985–1002, DOI: 10.1093/femsre/fuv026.
- (6) Zhang, G.; Meredith, T. C.; Kahne, D. On the Essentiality of Lipopolysaccharide to Gram-Negative Bacteria. Curr. Opin. Microbiol. 2013, 16, 779–785, DOI: 10.1016/j. mib.2013.09.007.
- (7) Tamm, L. K.; Arora, A.; Kleinschmidt, J. H. Structure and Assembly of β -Barrel Membrane Proteins. J. Biol. Chem. **2001**, 276, 32399–32402, DOI: 10.1074/jbc. R100021200.
- (8) Bos, M. P.; Robert, V.; Tommassen, J. Biogenesis of the Gram-Negative Bacterial Outer Membrane. Annu. Rev. Microbiol. 2007, 61, 191-214, DOI: 10.1146/annurev. micro.61.080706.093245.
- (9) Ried, G.; Hindennach, I.; Henning, U. Role of Lipopolysaccharide in Assembly of Escherichia Coli Outer Membrane Proteins OmpA, OmpC, and OmpF. J. Bacteriol. 1990, 172, 6048–6053, DOI: 10.1128/jb.172.10.6048-6053.1990.
- (10) Buehler, L. K.; Kusumoto, S.; Zhang, H.; Rosenbusch, J. P. Plasticity of Escherichia Coli Porin Channels. Dependence of Their Conductance on Strain and Lipid Environment. J. Biol. Chem. 1991, 266, 24446–50.
- (11) Okuda, S.; Sherman, D. J.; Silhavy, T. J.; Ruiz, N.; Kahne, D. Lipopolysaccharide Transport and Assembly at the Outer Membrane: The PEZ Model. Nat. Rev. Micro. 2016, 14, 337–345, DOI: 10.1038/nrmicro.2016.25.

- (12) Dong, H.; Fleming, G. R. Inhomogeneous Broadening Induced Long-Lived Integrated Two-Color Coherence Photon Echo Signal. J. Phys. Chem. B 2014, 118, 8956–8961, DOI: 10.1021/jp503045z, PMID: 25014005.
- (13) Rosenbusch, J. P. Characterization of the Major Envelope Protein from Escherichia coli. Regular Arrangement on the Peptidoglycan and Unusual Dodecyl Sulfate Binding. J. Biol. Chem. 1974, 249, 8019–8019.
- (14) Schindler, H.; Rosenbusch, J. P. Matrix Protein from Escherichia coli Outer Membranes Forms Voltage-Controlled Channels in Lipid Bilayers. Proc. Natl. Acad. Sci. 1978, 75, 3751–3755, DOI: 10.1073/pnas.75.8.3751.
- (15) Rocque, W. J.; Coughlin, R. T.; McGroarty, E. J. Lipopolysaccharide Tightly Bound to Porin Monomers and Trimers from Escherichia coli K-12. J. Bacteriol. 1987, 169, 4003–4010, DOI: 10.1128/jb.169.9.4003-4010.1987.
- (16) Holzenburg, A.; Engel, A.; Kessler, R.; Manz, H. J.; Lustig, A.; Aebi, U. Rapid Isolation of Ompf Porin-LPS Complexes Suitable for Structure-Function Studies. *Biochemistry* 1989, 28, 4187–4193, DOI: 10.1021/bi00436a010.
- (17) Ferguson, A. D.; Welte, W.; Hofmann, E.; Lindner, B.; Holst, O.; Coulton, J. W.; Diederichs, K. A Conserved Structural Motif for Lipopolysaccharide Recognition by Procaryotic and Eucaryotic Proteins. Structure 2000, 8, 585–592, DOI: 10.1016/s0969-2126(00)00143-x.
- (18) Arunmanee, W.; Pathania, M.; Solovyova, A. S.; Le Brun, A. P.; Ridley, H.; Baslé, A.; van den Berg, B.; Lakey, J. H. Gram-Negative Trimeric Porins Have Specific LPS Binding Sites That Are Essential for Porin Biogenesis. *Proc. Natl. Acad. Sci. USA* 2016, 113, E5034–E5043, DOI: 10.1073/pnas.1602382113.
- (19) Piggot, T. J.; Holdbrook, D. A.; Khalid, S. Conformational Dynamics and Membrane Interactions of the E. Coli Outer Membrane Protein FecA: A Molecular Dynamics

- Simulation Study. *Biochimica et Biophysica Acta (BBA) Biomembranes* **2013**, *1828*, 284–293, DOI: 10.1016/j.bbamem.2012.08.021.
- (20) Patel, D. S.; Re, S.; Wu, E. L.; Qi, Y.; Klebba, P. E.; Widmalm, G.; Yeom, M. S.; Sugita, Y.; Im, W. Dynamics and Interactions of OmpF and LPS: Influence on Pore Accessibility and Ion Permeability. *Biophys. J.* 2016, 110, 930–938, DOI: 10.1016/j.bpj.2016.01.002.
- (21) Patel, D. S.; Qi, Y.; Im, W. Modeling and Simulation of Bacterial Outer Membranes and Interactions with Membrane Proteins. *Curr. Opin. Struct. Biol.* **2017**, *43*, 131–140, DOI: 10.1016/j.sbi.2017.01.003.
- (22) Straatsma, T. P.; Soares, T. A. Characterization of the Outer Membrane Protein OprF of *Pseudomonas aeruginosa* in a Lipopolysaccharide Membrane by Computer Simulation. *Proteins* **2009**, *74*, 475–488, DOI: 10.1002/prot.22165.
- (23) Lee, J.; Pothula, K. R.; Kleinekathöfer, U.; Im, W. Simulation Study of OccK5 Functional Properties in *Pseudomonas aeruginosa* Outer Membranes. *J. Phys. Chem. B* **2018**, *122*, 8185–8192, DOI: 10.1021/acs.jpcb.8b07109.
- (24) Balusek, C.; Gumbart, J. Role of the Native Outer-membrane Environment on the Transporter BtuB. Biophys. J. 2016, 111, 1409–1417, DOI: 10.1016/j.bpj.2016.08.
 033.
- (25) Wu, E. L.; Fleming, P. J.; Yeom, M. S.; Widmalm, G.; Klauda, J. B.; Fleming, K. G.; Im, W. E. coli Outer Membrane and Interactions with OmpLA. Biophys. J. 2014, 106, 2493–2502, DOI: 10.1016/j.bpj.2014.04.024.
- (26) Fleming, P.; Patel, D.; Wu, E.; Qi, Y.; Yeom, M.; Sousa, M.; Fleming, K.; Im, W. BamA PORTA Domain Interacts with a Native Lipid Membrane Surface. *Biophys. J.* 2016, 110, 2698–2709, DOI: 10.1016/j.bpj.2016.05.010.
- (27) Jo, S.; Kim, T.; Iyer, V. G.; Im, W. CHARMM-GUI: A Web-based Graphical User

- Interface for CHARMM. *J. Comput. Chem.* **2008**, *29*, 1859–1865, DOI: 10.1002/jcc. 20945.
- (28) Jo, S.; Lim, J. B.; Klauda, J. B.; Im, W. CHARMM-GUI Membrane Builder for Mixed Bilayers and Its Application to Yeast Membranes. *Biophys. J.* 2009, 97, 50–58, DOI: 10.1016/j.bpj.2009.04.013.
- (29) Lee, J.; Patel, D. S.; Ståhle, J.; Park, S.-J.; Kern, N. R.; Kim, S.; Lee, J.; Cheng, X.; Valvano, M. A.; Holst, O. et al. CHARMM-GUI Membrane Builder for Complex Biological Membrane Simulations with Glycolipids and Lipoglycans. *J. Chem. Theory Comput.* **2018**, *15*, 775–786, DOI: 10.1021/acs.jctc.8b01066.
- (30) Lee, J.; Patel, D. S.; Ståhle, J.; Park, S.-J.; Kern, N. R.; Kim, S.; Lee, J.; Cheng, X.; Valvano, M. A.; Holst, O. et al. CHARMM-GUI Membrane Builder for Complex Biological Membrane Simulations with Glycolipids and Lipoglycans. *J. Chem. Theory Comput.* **2019**, *15*, 775–786, DOI: 10.1021/acs.jctc.8b01066.
- (31) Berendsen, H. J. C.; Postma, J. P. M.; van Gunsteren, W. F.; DiNola, A.; Haak, J. R. Molecular Dynamics with Coupling to an External Bath. J. Chem. Phys. 1984, 81, 3684–3690, DOI: 10.1063/1.448118.
- (32) Parrinello, M.; Rahman, A. Polymorphic Transitions in Single Crystals: A New Molecular Dynamics Method. J. Appl. Phys. 1981, 52, 7182–7190, DOI: 10.1063/1.328693.
- (33) Nosé, S. A Molecular Dynamics Method for Simulations in the Canonical Ensemble.

 Mol. Phys. 1984, 52, 255–268, DOI: 10.1080/00268978400101201.
- (34) Hoover, W. G. Canonical Dynamics: Equilibrium Phase-space Distributions. *Phys. Rev.* A 1985, 31, 1695, DOI: 10.1103/PhysRevA.31.1695.
- (35) Han, K.; Venable, R. M.; Bryant, A.-M.; Legacy, C. J.; Shen, R.; Li, H.; Roux, B.; Gericke, A.; Pastor, R. W. Graph—Theoretic Analysis of Monomethyl Phosphate Clustering in Ionic Solutions. *J. Phys. Chem. B* **2018**, *122*, 1484–1494, DOI: 10.1021/acs.jpcb.7b10730.

- (36) Pronk, S.; Páll, S.; Schulz, R.; Larsson, P.; Bjelkmar, P.; Apostolov, R.; Shirts, M. R.; Smith, J. C.; Kasson, P. M.; van der Spoel, D. et al. GROMACS 4.5: A High-throughput and Highly Parallel Open Source Molecular Simulation Toolkit. *Bioinformatics* 2013, 29, 845–854, DOI: 10.1093/bioinformatics/btt055.
- (37) Best, R. B.; Zhu, X.; Shim, J.; Lopes, P. E. M.; Mittal, J.; Feig, M.; MacKerell Jr, A. D. Optimization of the Additive CHARMM All-atom Protein Force Field Targeting Improved Sampling of the Backbone φ, ψ and Side-chain χ₁ and χ₂ Dihedral Angles. J. Chem. Theory Comput. 2012, 8, 3257–3273, DOI: 10.1021/ct300400x.
- (38) Klauda, J. B.; Venable, R. M.; Freites, J. A.; O'Connor, J. W.; Tobias, D. J.; Mondragon Ramirez, C.; Vorobyov, I.; MacKerell Jr, A. D.; Pastor, R. W. Update of the CHARMM All-atom Additive Force Field for Lipids: Validation on Six Lipid Types. J. Phys. Chem. B 2010, 114, 7830–7843, DOI: 10.1021/jp101759q.
- (39) Hatcher, E. R.; Guvench, O.; MacKerell, A. D. CHARMM Additive All-Atom Force Field for Acyclic Polyalcohols, Acyclic Carbohydrates, and Inositol. J. Chem. Theory Comput. 2009, 5, 1315–1327, DOI: 10.1021/ct9000608.
- (40) Guvench, O.; Hatcher, E.; Venable, R. M.; Pastor, R. W.; MacKerell, A. D. CHARMM Additive All-Atom Force Field for Glycosidic Linkages between Hexopyranoses. J. Chem. Theory Comput. 2009, 5, 2353–2370, DOI: 10.1021/ct900242e.
- (41) Hatcher, E.; Guvench, O.; MacKerell, A. D. CHARMM Additive All-Atom Force Field for Aldopentofuranoses, Methyl-aldopentofuranosides, and Fructofuranose. J. Phys. Chem. B 2009, 113, 12466–12476, DOI: 10.1021/jp905496e.
- (42) Guvench, O.; Greene, S. N.; Kamath, G.; Brady, J. W.; Venable, R. M.; Pastor, R. W.; Mackerell, A. D. Additive Empirical Force Field for Hexopyranose Monosaccharides. J. Comput. Chem. 2008, 29, 2543–2564, DOI: 10.1002/jcc.21004.
- (43) Wu, E. L.; Engström, O.; Jo, S.; Stuhlsatz, D.; Yeom, M. S.; Klauda, J. B.; Widmalm, G.; Im, W. Molecular Dynamics and NMR Spectroscopy Studies of E. Coli

- Lipopolysaccharide Structure and Dynamics. *Biophys. J.* **2013**, *105*, 1444–1455, DOI: 10.1016/j.bpj.2013.08.002.
- (44) Jo, S.; Wu, E. L.; Stuhlsatz, D.; Klauda, J. B.; Widmalm, G.; Im, W. Methods in Molecular Biology; Springer New York, 2015; Vol. 1273; pp 391–406, DOI: 10.1007/ 978-1-4939-2343-4_24.
- (45) Jorgensen, W. L.; Chandrasekhar, J.; Madura, J. D.; Impey, R. W.; Klein, M. L. Comparison of Simple Potential Functions for Simulating Liquid Water. J. Chem. Phys. 1983, 79, 926–935.
- (46) Darden, T.; York, D.; Pedersen, L. Particle Mesh Ewald: An N log(N) Method for Ewald Sums in Large Systems. J. Chem. Phys. 1993, 98, 10089–10092, DOI: 10.1063/ 1.464397.
- (47) Hess, B.; Bekker, H.; Berendsen, H. J. C.; Fraaije, J. G. E. M. LINCS: A Linear Constraint Solver for Molecular Simulations. J. Comput. Chem. 1997, 18, 1463–1472, DOI: 10.1002/(sici)1096-987x(199709)18:12<1463::aid-jcc4>3.3.co;2-1.
- (48) Waterhouse, A. M.; Procter, J. B.; Martin, D. M. A.; Clamp, M.; Barton, G. J. Jalview Version 2-a Multiple Sequence Alignment Editor and Analysis Workbench. *Bioinformatics* **2009**, *25*, 1189–1191, DOI: 10.1093/bioinformatics/btp033.
- (49) Varma, S.; Chiu, S. W.; Jakobsson, E. The Influence of Amino Acid Protonation States on Molecular Dynamics Simulations of the Bacterial Porin OmpF. *Biophys. J.* **2006**, 90, 112–123, DOI: 10.1529/biophysj.105.059329.
- (50) Ramakrishnan, M.; Pocanschi, C. L.; Kleinschmidt, J. H.; Marsh, D. Association of Spin-labeled Lipids with β-barrel Proteins from the Outer Membrane of Escherichia Coli. Biochemistry 2004, 43, 11630–11636, DOI: 10.1021/bi048858e.
- (51) Páli, T.; Bashtovyy, D.; Marsh, D. Stoichiometry of Lipid Interactions with Transmembrane Proteins–Deduced from the 3D Structures. *Protein Sci.* **2006**, *15*, 1153–1161, DOI: 10.1110/ps.052021406.

(52) Marsh, D. Stoichiometry of Lipid-Protein Interaction and Integral Membrane Protein Structure. Eur. Biophys. J. 1997, 26, 203–208, DOI: 10.1007/s002490050072.

Graphical TOC Entry

